BEAMFILLING CORRECTION STUDY FOR RETRIEVAL OF OCEANIC RAIN FROM PASSIVE MICROWAVE OBSERVATIONS

A Thesis

by

RUIYUE CHEN

Submitted to the Office of Graduate Studies of
Texas A&M University
in partial fulfillment of the requirements for the degree of

MASTER OF SCIENCE

May 2003

Major Subject: Atmospheric Sciences

BEAMFILLING CORRECTION STUDY FOR RETRIEVAL OF OCEANIC RAIN FROM PASSIVE MICROWAVE OBSERVATIONS

A Thesis

by

RUIYUE CHEN

Submitted to Texas A&M University
in partial fulfillment of the requirements
for the degree of

MASTER OF SCIENCE

Approved as to style and content by:

Thomas T. Wilheit (Chair of Committee)	Renyi Zhang (Member)
Kai Chang (Member)	Gerald R. North (Head of Department)

May 2003

Major Subject: Atmospheric Sciences

ABSTRACT

Beamfilling Correction Study for Retrieval of Oceanic Rain From Passive Microwave Observations (May. 2003)

Ruiyue Chen, B.S., M.S., Nanjing University of Aeronautics and Astronautics

Chair of Advisory Committee: Dr. Thomas T. Wilheit

Beamfilling error is one of the main error sources for microwave oceanic rainfall retrieval. An accurate beamfilling correction can improve the rainfall retrieval accuracy significantly. Quantitative understanding of the uncertainty of the Beamfilling Correction Factor (BCF) is very important for the understanding of the accuracy of microwave passive rainfall retrieval. Refinement of the calculation of the BCF and the estimation of BCF uncertainty are the main purposes of this thesis.

The characteristic of rainfall distribution is investigated. Quantitative understanding of the statistical characteristics of rainfall distribution provides an indication of the beamfilling error and the uncertainty of BCF in many ways.

Some refinements to the traditional BCF calculation algorithm are provided in this thesis. Scattering is included in the new algorithm. Also the BCF calculation only considers the cases within the useful dynamic range. These refinements make the BCF calculation closer to how it is used in the retrieval algorithm. The BCF based on the new algorithm should be more accurate.

The global BCF uncertainty and the local BCF uncertainty are estimated using the available A/C radar data. The results show that the uncertainty of BCF is much smaller

than expected, and also show that the BCF derived from a specific set of data can be used globally.

ACKNOWLEDGEMENTS

I would like to thank my advisor, Dr. Thomas T. Wilheit, for his guidance, encouragement, patience and financial support. Thanks also go to my other committee members: Dr. Renyi Zhang and Dr. Kai Chang for taking their time to be on my committee.

Many thanks go to my group-mates, both past and present: Alex Wang, for providing his program and dissertation about the beamfilling problem; Jun Huang, for helping me get started when I first joined the group; Richard Weitz, for his help with my written English; Kai Feng, Kyung-Wook Jin, Dong Heon Lee, Sungwook Hong and Jody L. Thomas –Stahle for their helpful discussions with me.

Special thanks to my wife Fangqing, my parents and my brothers for their love, understanding and encouragement.

This work was supported by the NASA TRMM and AQUA programs.

TABLE OF CONTENTS

LIST OF TABLES

LIST OF FIGURES

FIGURE Page

CHAPTER I

INTRODUCTION

Rainfall measurement over the ocean is very important in meteorology, hydrology and climatology. Among the methods to measure rainfall, Satellite Passive Microwave Rainfall Retrieval is widely used due to its large spatial coverage, its long temporal coverage and its direct interaction with hydrometeors.

There have been several spacecraft with microwave radiometers for rainfall measurement. These include the Nimbus 5 launched in 1972 and Nimbus 6 launched in 1975 with the Electrically Scanned Microwave Radiometers (ESMR), Nimbus 7 launched in 1978 with the Scanning Multi-channel Microwave Radiometer (SMMR), the Defense meteorological Satellite Program (DMSP) satellite series since 1987 with the Special Sensor Microwave/Imager (SSM/I), the Tropical Rainfall Measuring Mission (TRMM) satellite launched in 1997 with the TRMM Microwave Imager (TMI). To accommodate these rainfall measurement missions, a number of algorithms for retrieval of rainfall from passive microwave measurement have been developed. Current research topics for passive microwave rainfall measurement are refining and validating these algorithms.

Wilheit et al. (1977) developed a typical radiative transfer model to relate the rainfall over a field of view (FOV) with the satellite observed brightness temperature. Some algorithms based on this model (Wilheit et al. 1991) have been successfully used in many microwave rainfall retrieval studies. The output of this model can be

---

This thesis follows the style and format of the *Journal of Applied Meteorology*

summarized as a formula that expresses the relationship between the rainfall and the corresponding observed brightness temperature (R-T relationship). This formula contains an emission term and a scattering term. These two terms show the emission effect of rainfall on microwave radiation and the scattering effect of rainfall on microwave radiation respectively. An important assumption in the Wilheit et al. (1977) model is that the FOV of satellite microwave radiometer is completely covered by a uniform rainfall. However, the rainfall over a typical FOV is far from uniform because of the large FOV of a satellite microwave radiometer. At the same time, the R-T relationship derived from the Wilheit et al. (1977) model is very nonlinear. Hence the satellite observed brightness temperature and the average rain rate over the satellite FOV do not exactly satisfy the R-T relationship. This means the estimated average rain rate retrieved from a set of satellite observed brightness is not the true average rain rate over the FOV. The bias between the retrieved and true average rain rate is called beamfilling error. It is one of the main error sources for passive microwave rainfall retrieval. The factor used to correct the beamfilling error is called Beamfilling Correction Factor (BCF).

Many studies have been done to clarify the beamfilling problem. To get the BCF, it is necessary to understand how the rainfall is distributed. One method is to use aircraft (A/C) radar data, which have much higher resolution than the satellite microwave radiometer, to simulate satellite microwave observation and get the BCF for each simulated FOV. Then by averaging the BCFs of all simulated FOVs, an ensemble BCF may be obtained for global use. In principle, the BCF we get is only reasonable for the time and location of the data used, even then only in statistical sense. However, the available A/C radar data are limited as far as the satellite spatial coverage and time

coverage is concerned. The first aim of this paper is to clarify whether the BCF derived from a specific set of data can be used globally. The beamfilling problem will be investigated for two sets of A/C radar data during different seasons and in different locations. By comparing the two results, we can estimate to what degree the BCF derived from some specific set of A/C radar data can be used globally, and estimate the error induced by an inaccurate beamfilling correction. Also the uncertainty of BCF will be estimated.

The second aim of this paper is to estimate the impact of scattering term in the R-T relationship on the BCF calculation. Traditionally, the scattering term was dropped for the beamfilling error investigation because of its small contribution to the non-linearity of R-T relationship. Only the emission term was used in the simulation of satellite observation with A/C radar data. In fact, the scattering term does not affect the non-linearity much in the useful dynamic range of R-T relationship, however it acts as the dominant factor out of this range. Though the R-T relationship is always used in the useful dynamic range to retrieve rainfall, it is possible that some part of FOV is covered by the rainfall out of the dynamic range while the average rain rate over FOV is in the dynamic range. In this situation, the scattering term may still play an important role for BCF calculation. In this paper, the impact of the scattering term of R-T relationship on the BCF calculation will be investigated. Also the algorithm to simulate satellite observation with A/C radar data will be refined so that the simulation is closer to the reality.

The remaining part of this thesis is organized as follows. The background of microwave rainfall retrieval and previous work on the beamfilling problem are

introduced in chapter II. Chapter III describes the Airborne Rain Mapping Radar (ARMAR) data and the algorithm to process the data. In chapter IV, the characteristics of rainfall distribution and their relation with such issues as path averaging, FOV size are discussed. In chapter V, satellite rainfall observations are simulated with A/C radar data using two kinds of R-T relationships, one R-T relationship includes the emission term and scattering term while the other includes only the emission term. By comparing the results from the two R-T relationships, the impact of scattering term in R-T relationship to rainfall retrieval is evaluated. Also a formula is provided to relate BCF to FOV size and characteristic rain rate. Chapter VI investigates the uncertainty of BCF and shows that the BCF derived from a specific set of data can be used globally. Finally, a summary and conclusion are presented in chapter VII.

CHAPTER II

PASSIVE MICROWAVE OCEANIC RAINFALL MEASUREMENT AND BEAMFILLING PROBLEM

This chapter gives the background about the beamfilling problem and how to solve it. The principles of passive microwave oceanic rainfall measurement are introduced first, then some previous studies of beamfilling problem are summarized.

2.1 Principles of Passive Microwave Oceanic Rainfall Measurement

All substances emit electromagnetic energy because of the thermal motions of molecules and atoms. Brightness temperature is used to represent radiance. It is the temperature of a blackbody that could emit a given radiance. A blackbody is assumed to absorb and emit radiance perfectly. So its emissivity is 1. The emissivity for any substance other than blackbody is less than 1. In microwave region, the Plank Function can be approximated by the Rayleigh Jeans formula so that the radiance is proportional to the temperature of the substance. In this case, brightness temperature is the true temperature of the substance multiplied by the emissivity of the substance. An oceanic surface has a low and relatively unique emissivity in the microwave region, while liquid precipitation has a high emissivity. Hence there is a strong physical interaction between upwelling brightness temperature and rainfall over the ocean. Another effect of rainfall on microwave radiance is scattering. The scattering is negligible for small raindrops, but comparable with emission effect for large raindrops.

Wilheit et al. (1977) developed a radiative transfer model to relate the rain rate over the ocean and the satellite observed brightness temperature. The output of this model can be fitted as the following R-T relationship (Wilheit et al. 1991):

$$T(R) = T_0 + (T_1 - T_0)\left[1 - \exp\left(-\frac{R}{R_c}\right)\right] - a\sqrt{R} \qquad 2.1$$

Where $R_c = b/F^c$ and $T_0 = ta + tb \cdot F + tc \cdot F^2$. F is freezing level. r_c is characteristic rain rate. T_0 is the background temperature. T_1 , $ta, tb, tc,$ and a , b , c ,are determined by the frequency and view angle. For TMI, these parameters are given by Huang (2001) in table 1.

Table 1. Constant in R-T relationship (From Huang, 2001)

	10.65 GHz vertical channel	19.35 GHz vertical channel	21.3 GHz vertical channel	37.0 GHz vertical channel
ta	160.0	185.0	183.0	217.0
tb	1.75	-0.40	10.70	-4.00
tc	0.45	1.79	0.90	1.75
T_1	320.0	295.0	292.0	284.0
a	4.96	5.40	5.44	9.06
b	52.36	20.59	20.77	7.20
c	0.819	1.13	1.30	1.35

Fig. 1- Fig. 3 show the R-T relations for the TMI 10 GHz channel, the TMI 19 GHz channel and the TMI 37 GHz channel respectively. For all TMI channels, brightness temperature decreases as the rain rate increases over the high rain rate range because of the scattering of large raindrops. This makes the $T(R)$ relationship double valued for higher brightness temperatures. To avoid rainfall retrieval ambiguity, only the monotonic part of the R-T relation over the relatively low rain rate range, where the brightness temperature always increases as the rain rate increases, can be used for rainfall retrieval. This range is called useful dynamic range of a channel. For TMI, if the freezing level is assumed to be 4 km, the useful dynamic ranges are 0 mm/hr – 4 mm/hr for 37 GHz channel, 0 mm/hr – 14 mm/hr for 19 GHz channel, and 0 mm/hr – 50 mm/hr for 10 GHz channel.

2.2 Beamfilling Problem

The satellite microwave radiometer has large spatial coverage, but its spatial resolution is very low. Table 2 shows the spatial resolution for TMI.

Table 2. Spatial resolution for each TMI channel (From Huang, 2001)

Frequency (GHz)	Polarization	Spatial Resolution (km)
10.65	V	63×37
10.65	H	63×37
19.35	V	30×18
19.35	H	30×18
37	V	16×9
37	H	16×9

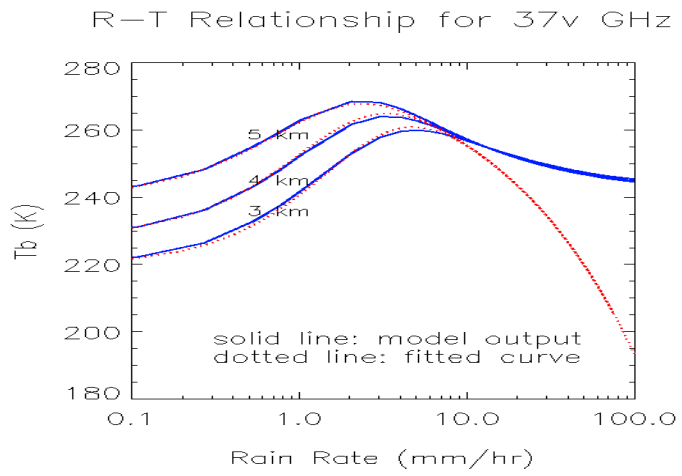

Fig. 1 R - T relationship for TMI 37 GHz channel (from Huang, 2001)

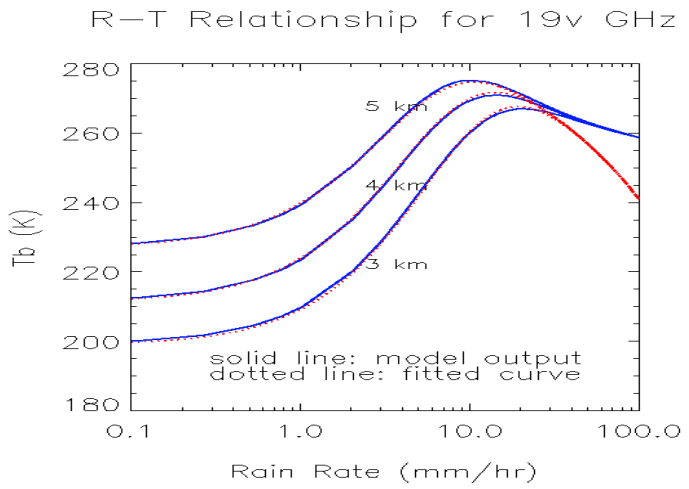

Fig. 2 Same as Fig. 1 except for TMI 19 GHz channel

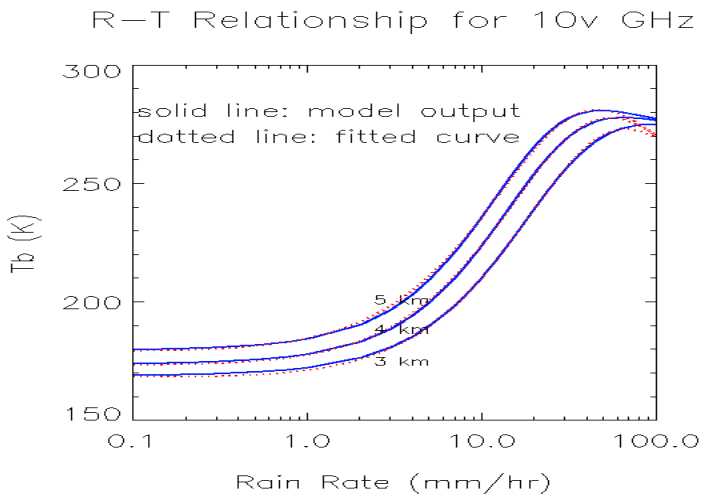

Fig. 3 Same as Fig. 1 except for TMI 10 GHz channel

The highest resolution for TMI channels which can be applied to rainfall retrieval is 16×9 km. The rainfall must be non-uniformly distributed in such a FOV size unless there is no rain over the FOV. At the same time, the R-T relationship derived from the radiative transfer Model of Wilheit et al. (1977) is nonlinear. Hence the satellite observed brightness temperature and the average rain rate do not exactly satisfy the R-T relationship. This means the estimated average rain rate retrieved from a set of satellite observed brightness temperature is not the true average rain rate over the FOV. The bias between the retrieved and true average rain rate is called beamfilling error. The coefficient used to correct this error is called the Beamfilling Correction Factor (BCF).

Usually, the scattering term is dropped for BCF investigations because of its small contribution to the non-linearity of R-T relationship. Chiu et al. (1990) derived a formula to relate the BCF to the characteristic rain rate and the statistical character of the rain rate as follows:

$$BCF \approx 1 + \frac{1}{2}\frac{Var(R)}{R_e}\frac{T''(R_2)}{T'(R_3)} \qquad 2.2$$

Where R_e is the estimated rain rate corresponding to the satellite observed brightness temperature, R_c is the characteristic rain rate and $Var(R)$ is the variance of the rain rate over the FOV. The last term $T''(R_2)/T'(R_3)$ arises from the expansion of the R-T relationships. It is approximated as $1/R_c$ to simplify the analysis and the formula becomes as follows:

$$BCF \approx 1 + \frac{1}{2}\frac{Var(R)}{R_e}\frac{1}{R_c} \qquad 2.3$$

This approximation sacrifices precision significantly. Fig. 4 shows the comparison between this formula and real data BCF calculations. As will be discussed in chapter V, the real data calculation does not include the scattering term in the R-T relationship either. The comparison shows that formula 2.3 overestimates BCF, especially for the cases with large rain rate variance. Hence we may add a variable C to formula 2.3 as:

$$BCF = 1 + \frac{1}{2}\frac{Var(r)}{R_e}\frac{1}{R_c}C \qquad 2.4$$

For most cases, the adjustment C is less than 1 and decreases as variance of rain rate increases.

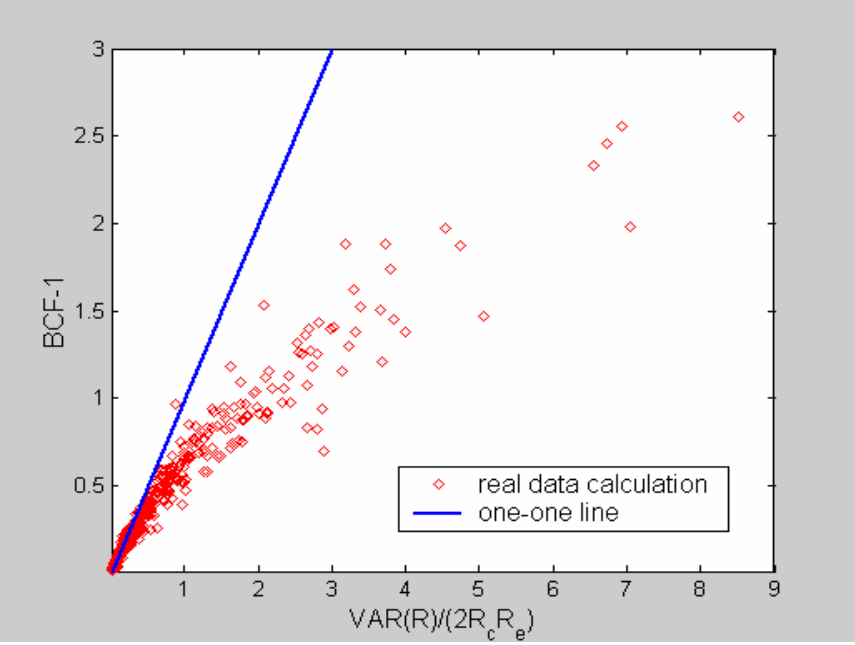

Fig. 4 Comparison between Chiu's BCF formula and real data BCF calculations

Some important characteristics of BCF can be obtained from Chiu's BCF formula.

1) BCF is always greater than 1.
2) BCF increases as the variance of rain rate increases.
3) BCF is negatively related to characteristic rain rate.

Ha and North (1995) studied beamfilling error for various rainfall distribution models. The BCF increases as FOV size increases for their rainfall distribution model, but there is an upper bound.

All of these theoretical studies help us understand the characteristics of the beamfilling problem. However they can not give BCF quantitatively because it is impossible to know the variance of rain rate theoretically. Usually high-resolution data from other rainfall measurement instruments are used to simulate satellite radiometer observations and estimate BCF. Wang (1996) showed that, to simulate the satellite observation, the rain rate should be averaged along the satellite viewing direction as reflected off the surface. His results show that proper three-dimensional averaging significantly reduced the beamfilling error compared with the calculation in two horizontal dimensions.

On the basis of the previous studies, this paper tries to make progress on the following two topics:

1) The impact of scattering on BCF.
2) Quantitatively estimating the uncertainty of BCF.

CHAPTER III

DATA PREPARATION

In this chapter, the Airborne Rain Mapping Radar (ARMAR) is introduced. Its three dimensional rainfall data can be used to simulate satellite radiometer observations and estimate BCF because of its high resolution. The raw data of ARMAR is rainfall reflectivity. Some algorithms to retrieve rain rate effectively from reflectivity are also discussed in this chapter.

3.1 Introduction of ARMAR

ARMAR (Durden et al. 1994) was developed by NASA/JPL for the purpose of supporting spaceborne rain radar systems. It flies on the NASA Ames DC-8 aircraft. ARMAR is operated using the geometry and frequency of the Tropical Rain Measuring Mission (TRMM) precipitation radar. ARMAR therefore operates at 13.8 GHz and has the cross-track scanning geometry shown in Fig. 5. Its main characteristics are shown in Table 3. Its range resolution is 60m(3db width) and its surface horizontal resolution is 800m from an altitude of 12km. Because these two parameters are much smaller than those of the TRMM radiometer and radar, the ARMAR data are suitable for investigating the beamfilling problem for TRMM.

The ARMAR system was deployed during the TOGA/COARE and KWAJEX field experiments. TOGA/COARE took place in the western Pacific in early 1993. KWAJEX was on the Kwajalein Atoll, Republic of the Marshall Islands, in the central Topical

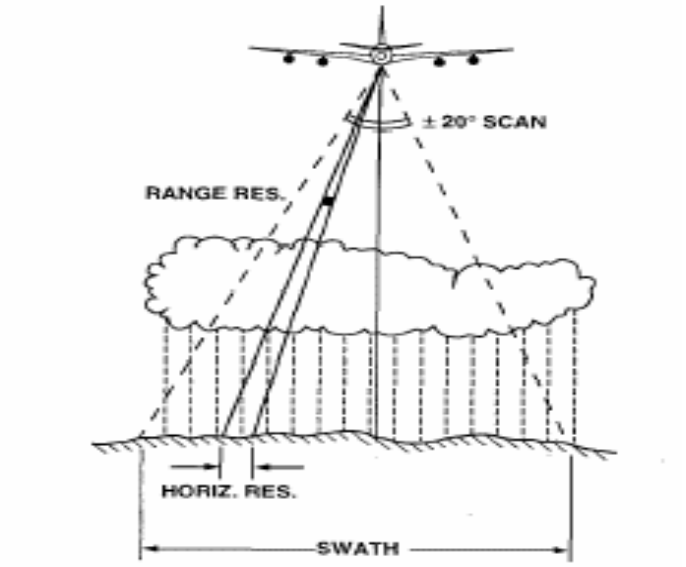

Fig. 5 ARMAR observational geometry (from Durden et al., 1994)

Table 3 ARMAR system parameters (from Durden et al., 1994)

Range resolution (-6 dB width)	80m
Surface horizontal resolution (12 km altitude)	800m
Swath width	9 km
Frequency	13.8 GHz
Polarization	HH,VV,HV,VH

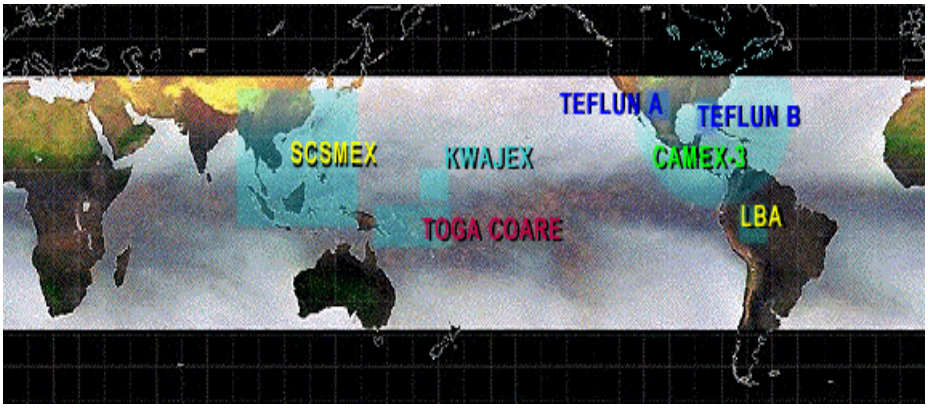

Fig. 6 Location of TRMM validation experiments

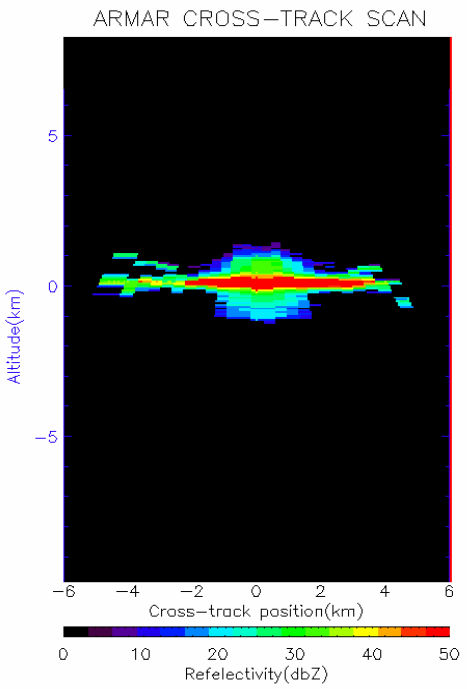

a) clear

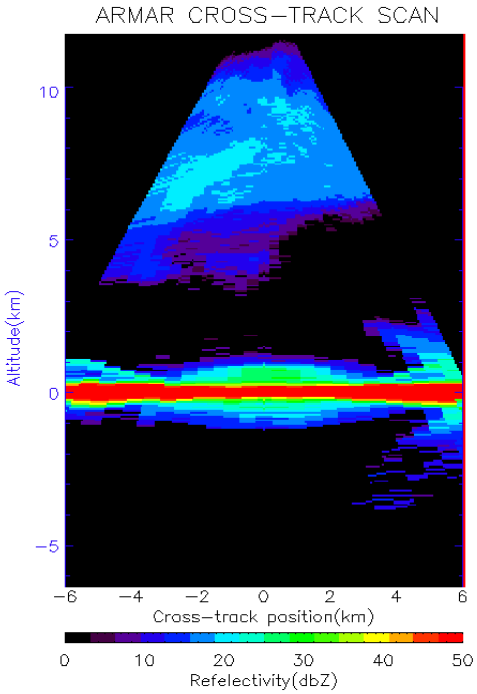

b) very light rain

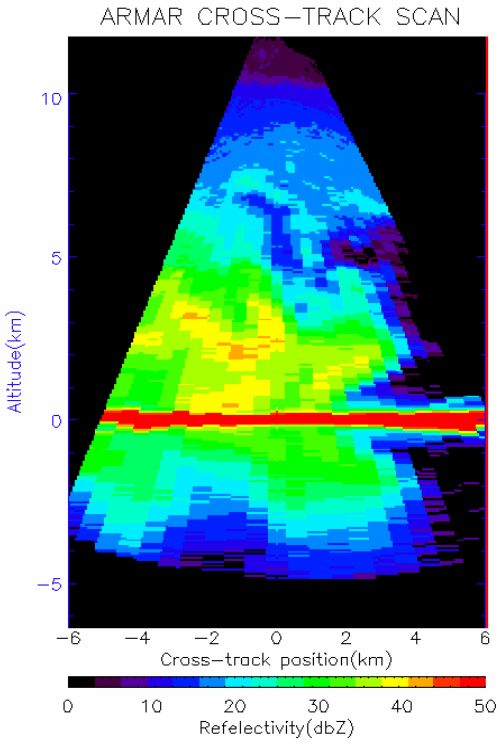

c) convective rain

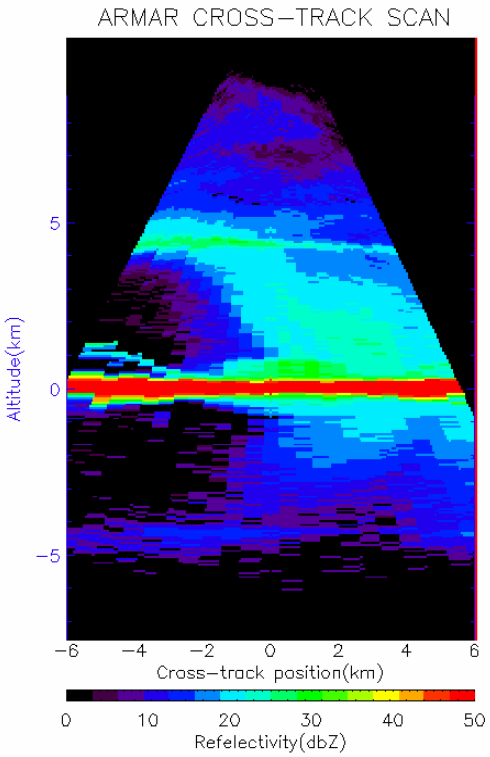

d) stratiform rain

Fig. 7 ARMAR cross-track scan profiles

Pacific during the summer of 1999. Fig. 6 shows the locations of the two field experiments. The characteristics of ARMAR in TOGA/COARE were the same as displayed in Table 3, except in KWAJEX, the cross-track scan is from –25° to 25°, which makes the scan swath 11 km from an altitude of 12km. The primary goal of ARMAR in these two experiments was the measurement of the three-dimensional structure of rainfall. Its measurement covers a wide variety of storm types, including convective and stratiform precipitation. Fig. 7 displays typical reflectivity profiles from the ARMAR cross-track scan. Such issues as sea surface return, mirror image and freezing level for stratiform rain are clearly displayed in these figures.

3.2 ARMAR Data Processing

1. Sidelobe of Sea Surface Return

Fig. 7a shows a cross scan of ARMAR in clear air. In this figure, a region of high-reflectivity near the sea surface return can be seen. This is the range sidelobe of the sea surface return and its mirror image. This range sidelobe is caused by the pulse compression of ARMAR (Tanner et al., 1994), which can improve range resolution significantly. Fig. 8 shows the structure of the range sidelobe for a nadir ARMAR beam. Because the sidelobe power varies significantly, it is hard to remove the sidelobe accurately. In this paper, to avoid the influence of this range sidelobe, the data below 1km altitude are not used.

2. Attenuation Correction

Attenuation refers to energy losses due to absorption and scattering between the radar and the target (Hitschfeld and Bordan, 1953). Due to attenuation, the radar

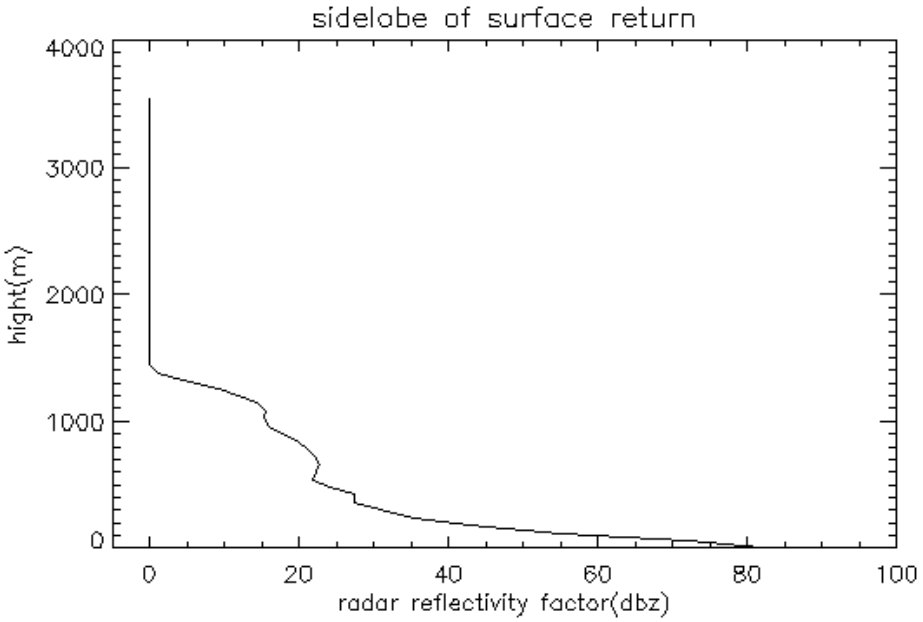

Fig. 8 Range sidelobe of sea surface return for nadir ARMAR beam

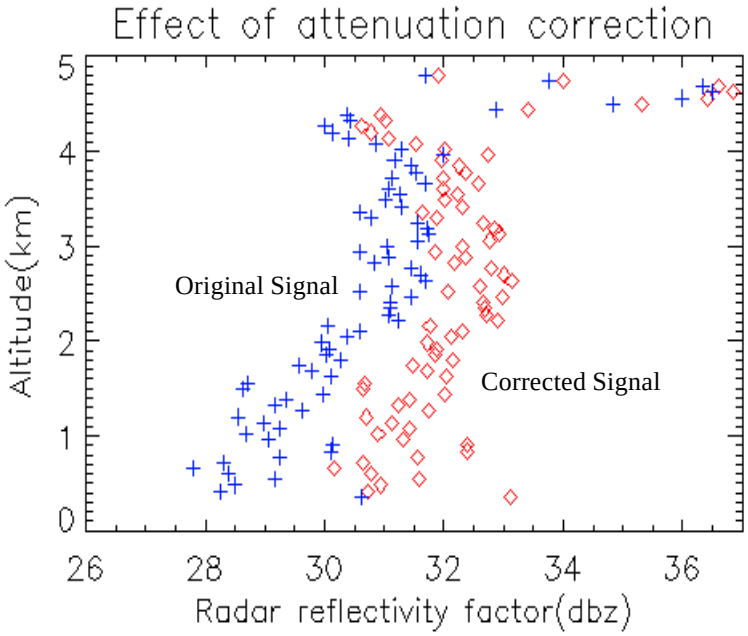

Fig. 9 Effect of attenuation correction to a nadir ARMAR beam

measured reflectivity of the target is smaller than the true value. The relationship between the attenuation k and the rainfall reflectivity Z is:

$$k = aZ^b \tag{3.1}$$

where k is in dB/km and Z is in mm^6/m^3.

The attenuation is very serious for high frequencies. For spaceborne radar, high frequencies must be used to improve resolution. ARMAR uses the frequency of TRMM radar and operates at 13.8 GHz. Hence attenuation correction must be done to ARMAR data to obtain the true reflectivity of targets. In this paper, the attenuation correction method from Iguchi and Meneghini (1994) is used. The corrected reflectivity, $Z_a(r)$, is given by:

$$Z_a(r) = Z_m(r)\left\{A_s^b + eq[S(r_s) - S(r)]\right\}^{-1/b} \tag{3.2}$$

where $Z_m(r)$ is the measured reflectivity. $A_s = Z_m(r_s)/Z(r_s)$ is the attenuation factor at the sea surface. q is $0.2b\ln(10)$. $S(r) = \int_0^r aZ_m^b(r)dr$ is the integration of attenuation from the radar to the target based on measured reflectivity. e is the correction factor. For heavy rain, which is indicated by $qS(r_s) > 1$,

$$e = \left(1 - A_s^b\right)/qS(r_s)$$

For light rain, which is indicated by $qS(r_s) \le 1$,

$$e = 2 - A_s^b - qS(r_s)$$

The coefficients a and b are from formula 3.1. Fig. 9 shows the attenuation correction effect to a nadir ARMAR beam. The attenuation correction makes the rainfall reflectivity along this nadir beam more uniformly distributed in the vertical dimension.

3. Z-R Relationship

The Reflectivity-Rain Rate relationship (Z-R relationship) for rainfall is determined by the rain drop size distribution. Marshall and Palmer (1948) found an exponential shape fits the measured raindrop spectra reasonably well. The Marshall-Palmer raindrop size distribution is widely used. Marecal et al. (1997) used Marshall-Palmer distribution to calculate Z-R relation for ARMAR. The result was $Z = 265.5R^{1.614}$. They also used microphysical data to adjust the Z-R relation for convective rain in TOGA/COARE, which contains a large number of small size raindrops. The result was $Z = 83.1R^{1.614}$. Alex Wang (1996) applied $Z = 176R^{1.45}$ to ARMAR data collected in TOGA/COARE. Fig. 10 shows a comparison of these Z-R relations. The Z-R relation that Alex Wang used is close to the Z-R relationship from the Marshall-Palmer raindrop size distribution for low rain rates, and is close to the Z-R relationship of TOGA/COARE convective rain for high rain rates. The $Z = 176R^{1.45}$ relationship is used in this paper.

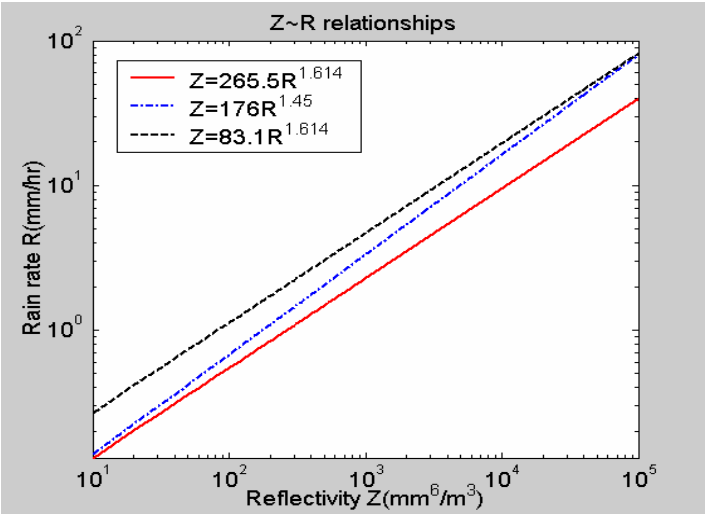

Fig. 10 Different Z~R relationships

CHAPTER IV

THE CHARACTERISTICS OF RAINFALL DISTRIBUTION

The highly variable distribution of rain rate is one of the key factors that determine beamfilling error. Quantitative understanding of the variance of rain rate over FOV means quantitatively understanding of the BCF. In this chapter, the characteristics of rain rate distribution are statistically summarized using A/C radar data. Its relation with such issues as path averaging and FOV size are also discussed.

4.1 Path-averaging

Wang (1996) showed that path averaging could reduce BCF significantly. This changed the traditional opinion that BCF is very large. In the following, the impacts of path averaging on rain rate distribution are shown in detail.

A satellite microwave radiometer receives the integrated radiation along the satellite viewing direction as reflected off the surface. So path-averaging should be done when A/C radar data are used to simulate satellite radiometer observations. Because the rain rate is nearly uniformly distributed in the vertical dimension, path averaging can strengthen the correlation of rain rate in the spatial domain. For TMI, the viewing angle is 53°. This means that the rain rate over more than 10 km in the horizontal dimension should be involved in path averaging if the freezing level is assumed to be 4 km.

Fig. 11 shows horizontally sliced rain and path-averaged rain at the same location and time. The path averaged rain is much more uniformly distributed than horizontally sliced rain. The standard deviation (STD) for the horizontally sliced rain is 11 mm/hr, but

only 5 mm/hr for the path averaged rain. According to formula 2.2, path averaging can reduce beamfilling error by a factor of 4 for this case. The average rain rate of the horizontally sliced rain is 9 mm/hr, while the average rain rate of the path averaged rain is 8.1 mm/hr. This is consistent with the rain rate being nearly uniformly distributed in the vertical dimension, while the rain rate can be very non-uniformly distributed over the horizontal dimension.

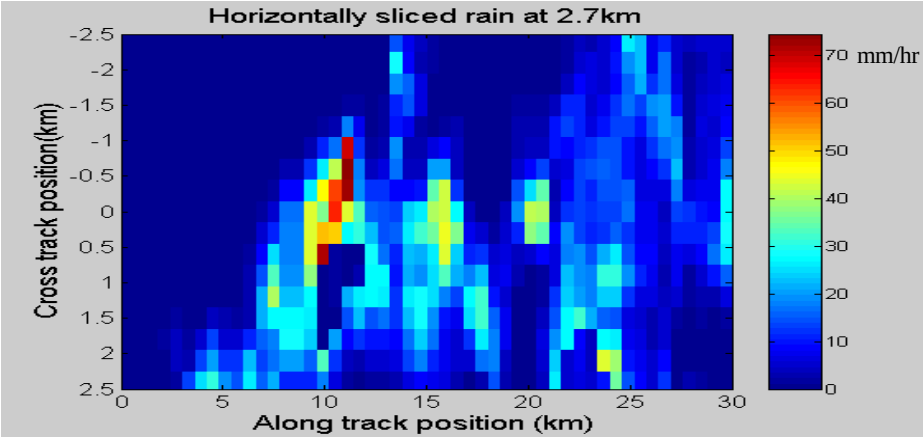

a) Horizontally Sliced Rain at 2.7 km

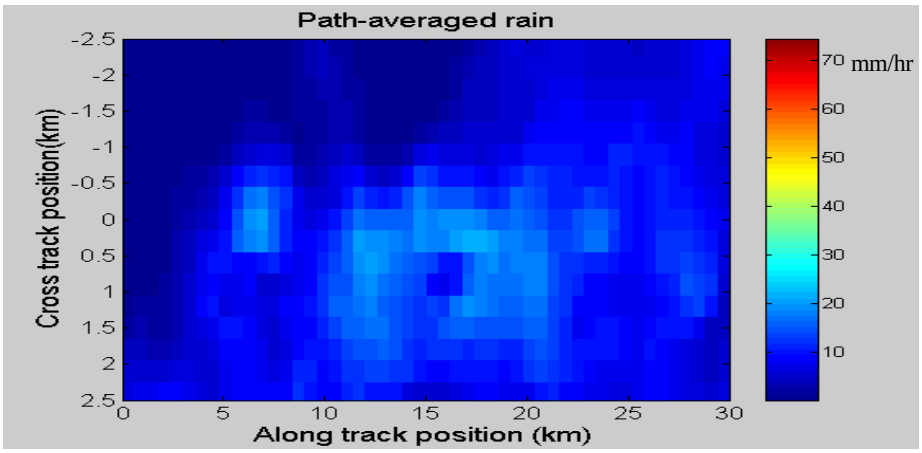

b) Path Averaged Rain

Fig. 11 Effect of path averaging

To quantitatively understand the impact of path averaging on rain rate variance, TMI FOVs are simulated using ARMAR data from KWAJEX. The STD of rain rate is calculated over simulated TMI FOVs. TMI FOV sizes are 16 km for 37GHz, 30km for 19GHz and 63km for 10Ghz channel. The STDs are calculated with the horizontally sliced rain and with the path averaged rain. The results are shown in Fig. 12-Fig. 14.

It is well known that the STD of rain rate increases as the mean rain rate increases. The regression results between the STD and the mean rain rate are shown in Table 4. The STD of rain rate can be statistically expressed as $s = kR^a$, where s is the STD of rain rate and R is the average rain rate over the FOV. The difference of s between path averaged rain and horizontally sliced rain is mainly represented by the difference of k. If the difference of a is not considered, in average, compared with horizontally sliced rain, path averaging can reduce STD of rain rate by a factor of 1.9 for 16 km FOV size, by a factor of 1.6 for 30 km FOV size, and by a factor of 1.7 for 63 km FOV size. According to formula 2.3, path averaging can reduce beamfilling error by a factor of 2 to 4 in average. In the following discussion, rain rate refers to path averaged rain rate based on TMI geometry if not otherwise specified.

Table 4 The impact of path averaging on STD of rain rate

FOV size	STD for horizontal slice rain	STD for path averaged rain
16 km	$s = 1.25R^{0.65}$	$s = 0.67R^{0.62}$
30 km	$s = 1.47R^{0.67}$	$s = 0.87R^{0.63}$
63 km	$s = 1.78R^{0.61}$	$s = 1.05R^{0.64}$

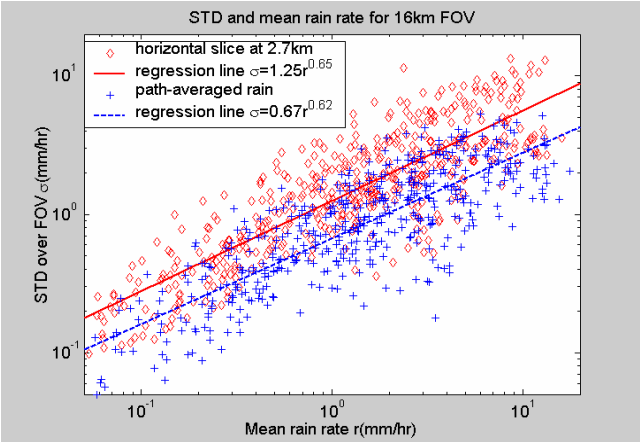

Fig. 12 The impact of path-averaging on rain rate variance for 16 km FOV

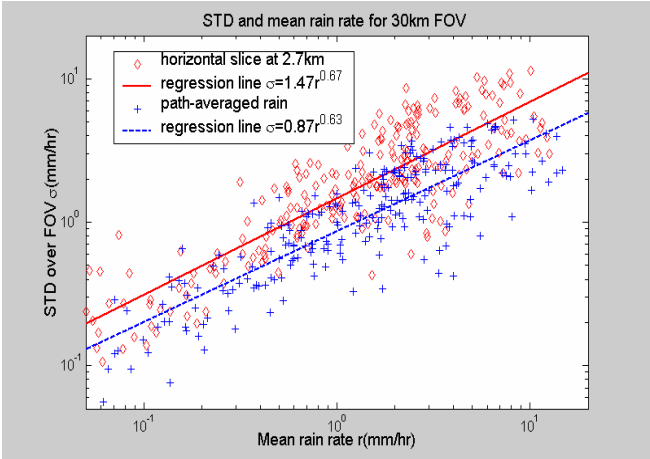

Fig. 13 Same as Fig 12 except for 30 km FOV

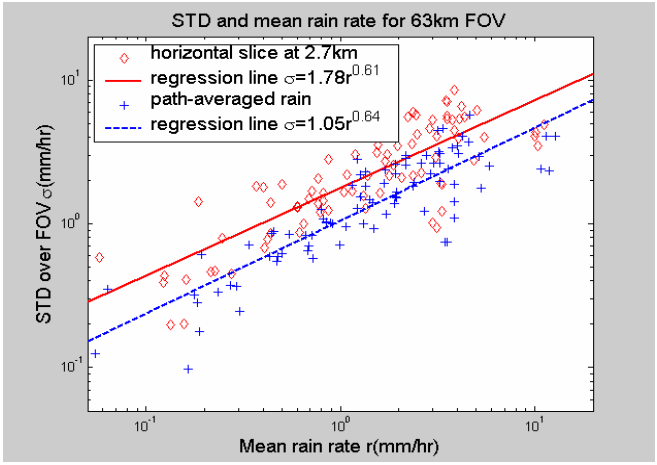

Fig. 14 Same as Fig. 12 except for 63 km FOV

In Fig. 11, there are some extremely heavy rain rates, as large as 70 mm/hr, in the horizontally sliced rain. These extreme rain rates usually are out of the usable dynamic range of a channel. Due to their scattering, these extreme rain rates may contribute the same amount of radiation as some light rain rates. The existence of extremely heavy rain can introduce unacceptable error into the rainfall retrieval. Fortunately, path averaging can smooth the rain along its viewing path and eliminate the extreme rain rates remarkably well. Fig. 15 displays this by comparing the histogram of path-averaged rain with that of horizontally sliced rain. Both histograms are calculated using ARMAR data from KWAJEX

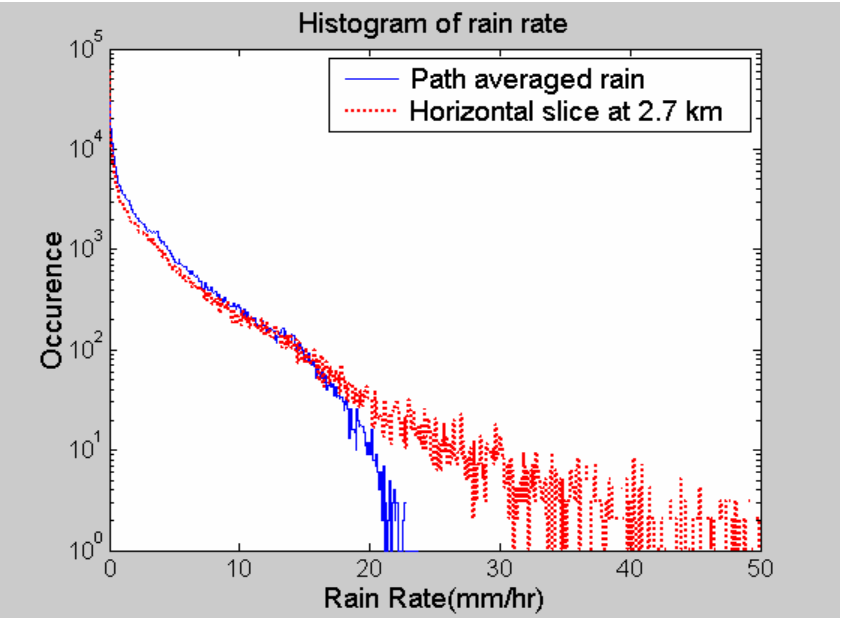

Fig. 15 Comparison of rain rate histograms between horizontally sliced rain and path averaged rain

4.2 The Impact of FOV Size on the STD of Rain Rate

Generally speaking, the STD of rain rate increases as the FOV size increases. Fig.12 – Fig.14 are the real data calculation results of rain rate STD for a 16 km FOV, a 30 km FOV and a 63 km FOV. The same calculation is also done for a 48 km FOV. The regression statistically summarizes the STD of rain rate as:

For 16 km FOV $s = 0.67R^{0.62}$ 3.1

For 30 km FOV $s = 0.87R^{0.63}$ 3.2

For 48 km FOV $s = 0.95R^{0.63}$ 3.3

For 63 km FOV $s = 1.05R^{0.64}$ 3.4

Where s is the standard deviation, and R is the mean rain rate over the FOV.

If the STD is expressed as $s = kR^a$, the change of s as the FOV size changes is mainly represented by a change of k. Fig. 16 shows the relationship between STD of rain rate and FOV size. The following formula fits the real calculation results well.

$$s = 0.56\log_{10}(fov)R^{0.63} \qquad fov \le 63km \qquad 3.5$$

where fov is the FOV size in the longer dimension. When the FOV size approaches $60\,km$, the STD increases very slowly as the FOV size continues to increases. This is consistent with the saturation phenomena described by Wang (1996), Ha and North (1995) and Chiu (1990). As they point out, there is an upper bound for the beamfilling error as the FOV increases.

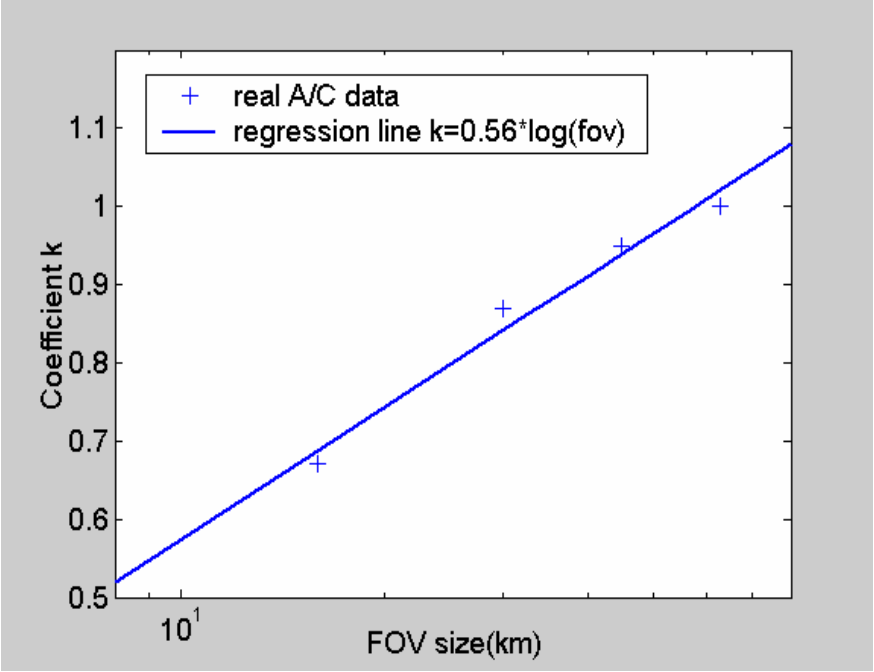

Fig. 16 The relationship between STD of rain rate and FOV size

4.3 Limitation of ARMAR Cross-track Scan Swath and its Impact

The ARMAR cross-track scan is from –20° to 20° in the TOGA/COARE experiment, and from –25° to 25° in KWAJEX experiment. This means that the scan swath is 7.2 km at the sea surface for TOGA/COARE and is 9.3 km at the sea surface for KWAJEX if the aircraft altitude is 10 km. To simulate satellite observations accurately and maximize the path averaging effect, only the data within the scan swath at the freezing level can be used. The ARMAR scan swath at the freeing level is about 4 km for TOGA/COARE and is about 5 km for KWAJEX if the aircraft altitude is assumed to be 10 km and the freezing level is assumed to be 4.5 km.

When the aircraft flies straight, the ARMAR data in the along –track direction can simulate any satellite FOV size. Usually the ARMAR data in the along-track direction are used to fill the longer dimension of the satellite FOV. However the available ARMAR cross-track scan swath is only about 4 km or 5 km, which is much shorter than the satellite FOV size in the shorter dimension. From Table 2 in chapter II, for TMI, the FOV size in the shorter dimension is 9 km for the 37 GHz channel, 18 km for the 19 GHz channel and 37 km for the 10 GHz channel. This is the main disadvantage of simulating satellite radiometer observations with A/C radar data. To understand how this disadvantage affects the simulation, the STD of rain rate is calculated for a 1 km cross-track scan swath. This STD result is compared with the same calculation result for a 5 km cross-track scan swath. Both calculations use ARMAR data collected in KWAJEX.

The results marked as “path averaged rain” in Fig. 12 – Fig. 14 are the calculation results for a 5 km cross-track scan swath and the regressions of these results are shown as

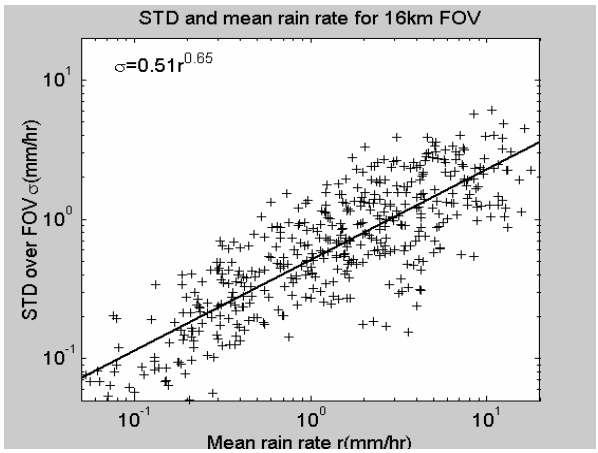

Fig. 17 Standard deviation of rain rate for a 1 km scan swath and 16km along-track length

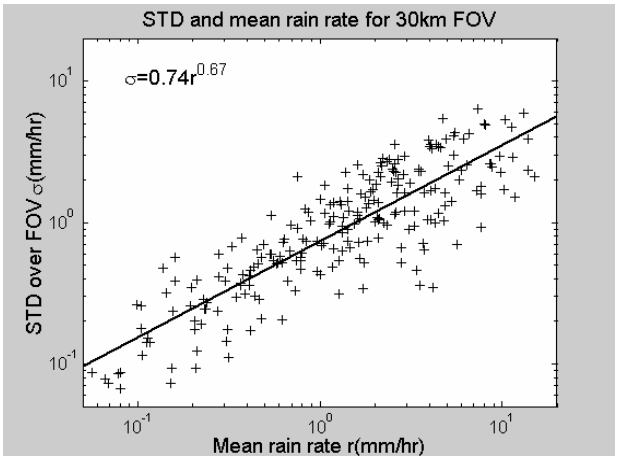

Fig. 18 Same as Fig. 17 except the along-track length is 30 km

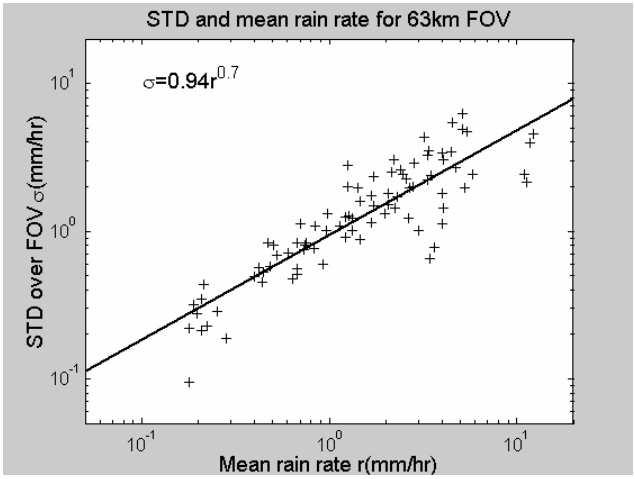

Fig. 19 Same as Fig. 17 except the along-track length is 63 km

equation 3.1, 3.2 and 3.4. The calculation results for a 1 km cross-track scan swath are shown in Fig. 17, Fig. 18 and Fig. 19. The regression results are:

For 16 km along-track length $s = 0.51R^{0.65}$ 3.5

For 30 km along-track length $s = 0.74R^{0.67}$ 3.6

For 63 km along-track length $s = 0.94R^{0.7}$ 3.7

The results do not change much compared with 3.1, 3.2 and 3.4. There are two reasons for this. One is that the along-track length is much longer than the cross-track length. The other is that the path averaging introduces a scale length and smoothes the rain rate distribution over FOV. Also, the saturation effect, mentioned in §3.2, determines the STD of rain rate would not increase much, maybe even decrease, as the cross-track scan swath increases if the along-track length is long enough. Hence the difference between the cross-track scan swath of ARMAR and the satellite FOV size in the shorter dimension should not significantly affect the effectiveness of the simulation.

4.4 Rain Rate Distribution Comparison Between KWAJEX and TOGA/COARE

The rain rate distribution is the only variable factor that determines the uncertainty of beamfilling error for a microwave channel. To understand the uncertainty of beamfilling error, the uncertainty of the rain rate distribution should be investigated first. Although the rain rate distribution varies significantly as the time and location of rainfall changes, most of the variations should be in a limited range. Both in TOGA/COARE and KWAJEX, the ARMAR data collected cover a wide variety of rain types. These two experiments are during different seasons and in different locations. By investigating rain

rate distribution characteristics for these two ARMAR data sets and comparing the results, the statistical homogeneity of rainfall can be illuminated.

According to the experiment catalogs (JPL, 1993, 1999), there are more convective rain storms in TOGA/COARE, while there is more stratiform rain in KWAJEX. Fig. 20 compares the rain rate histogram from the TOGA/COARE ARMAR data with that from the KWAJEX ARMAR data. The two results are very similar. The smoothing effect of path averaging contributes significantly to the similarity. However there is still some difference between the rain rate histograms of the two experiments. The comparison shows TOGA/COARE contains more light rain and heavy rain, while KWAJEX contains more medium rain. This is consistent with what the data catalog recorded.

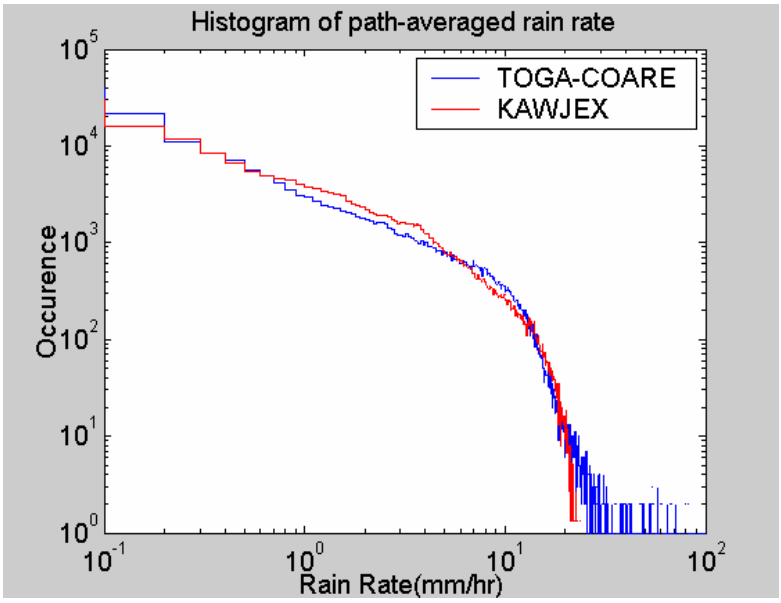

Fig. 20 Comparison of rain rate histograms between TOGA/COARE and KWAJEX

The variance of rain rate over the FOV is the most important characteristic of rain rate distribution for the beamfilling problem. The STD of rain rate is calculated with KWAJEX ARMAR data and with TOGA/COARE ARMAR data. Fig. 16 – Fig. 18 show comparisons between the two results. Table 5 shows the regressions of the two results.

Table 5. Comparison of rain rate STD between TOGA/COARE and KWAJEX

FOV size	STD for TOGA/COARE	STD for KWAJEX
16 km	$s = 0.50R^{0.73}$	$s = 0.67R^{0.62}$
30 km	$s = 0.72R^{0.73}$	$s = 0.87R^{0.63}$
63 km	$s = R^{0.77}$	$s = 1.05R^{0.64}$

From Fig. 21 – Fig. 23, for all TMI FOV sizes, the rain rate STD calculation results are similar for the two experiments, except that there are a few extreme cases of very high and very low rain rates in TOGA/COARE. These extreme cases dominate the difference of the STD for the two experiments, which can be seen in table 5.

Generally speaking, the comparisons show that, after path averaging, the statistical characteristics are quite similar for rainfall during different times and in the different locations, if the rainfall covers various types of rain.

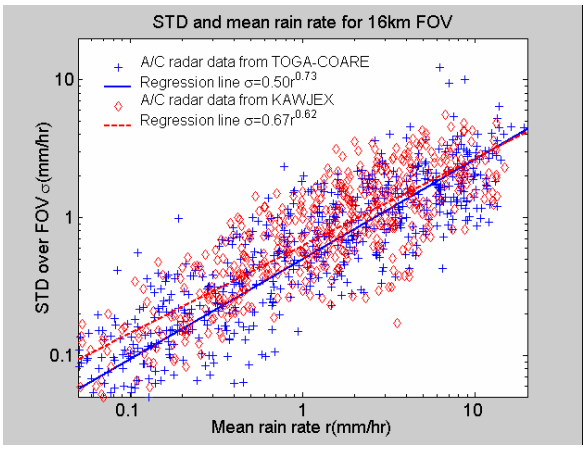

Fig. 21 Comparison of rain rate distribution between TOGA/COARE ARMAR data and KWAJEX ARMAR data for a 16 km FOV size

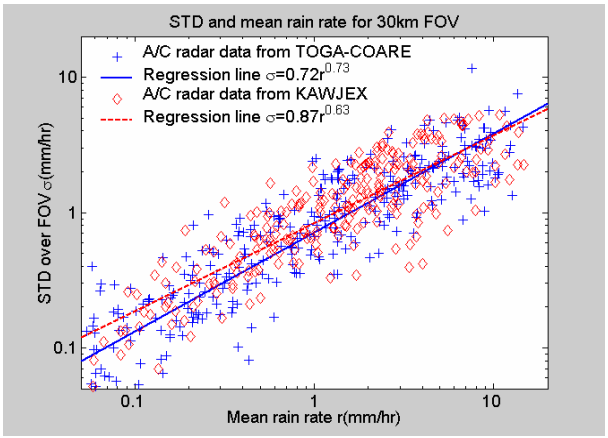

Fig. 22 Same as Fig. 21 except for a 30 km FOV size

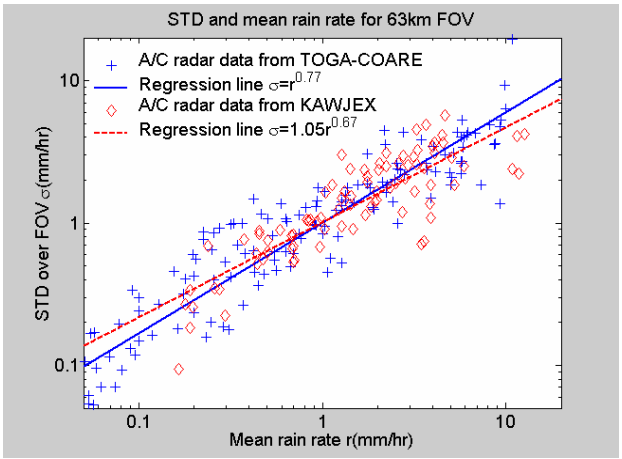

Fig. 23 Same as Fig. 21 except for a 63 km FOV size

CHAPTER V

EFFECT OF SCATTERING ON THE BEAMFILLING CORRECTION

All previous investigators neglected the scattering effect of rainfall for beamfilling error estimation because of its complicated but small contribution to the non-linearity of the R - T relationship. However the scattering effect acts as a dominant factor for heavy rain that is out of the useful dynamic range. This chapter analyzes the impact of scattering on beamfilling error. Based on this analysis, some refinements are provided to make the beamfilling error estimation closer to the reality.

5.1 Impact of Scattering on Beamfilling Error

In chapter II, scattering was mentioned to be negligible for very light rain, but comparable with emission for large raindrops. Fig. 1 – Fig. 3 show that large rain rates, out of the useful dynamic range, can have the same brightness temperature as lower rain rates in the useful dynamic range. Hence the large rain rate, out of the useful dynamic range, looks like a low rain rate in the useful dynamic range for microwave rainfall retrieval. In reality, if a rain rate is out of the useful dynamic range for some channel, the retrieval of this rain rate depends on the lower frequency channel, which has a larger useful dynamic range, but the accuracy is lower. However it is possible that some part of a FOV is covered by the rainfall out of the useful dynamic range while the average rain rate over FOV is in the useful dynamic range. Scattering can reduce the retrieved rain rate of this FOV significantly because the rainfall out of the useful dynamic range appears to

be some light rainfall. Therefore, the scattering term can increase beamfilling error for this FOV.

For TMI, if the freezing level is assumed to be 4.5 km, the useful dynamic ranges are 0 mm/h – 3 mm/h for the 37 GHz channel, 0 mm/h – 12 mm/h for the 19 GHz channel, and 0 mm/h – 50 mm/h for the 10 GHz channel. According to the rain rate histogram in Fig. 11, after path averaging, most rain rates are smaller than 50 mm/h, a small portion of rain rates are larger than 12 mm/h and many are larger than 3 mm/h. Hence scattering is expected to increase beamfilling error significantly for the 37 GHz channel, increase beamfilling error slightly for the 19GHz channel and have no obvious effect for the 10 GHz channel.

To show the impact of scattering on beamfilling error, satellite observations of TMI channels are simulated using ARMAR data from KWAJEX. Two types of R-T relations are applied to the simulation. One includes both the scattering term and the emission term, while the other includes only the emission term. Fig. 24 – Fig. 26 compare the results of these two simulations. For all channels, the main differences are in the low and high ends of the useful dynamic range. Certainly there is a big difference out of the useful dynamic range, but this region is not useful for rainfall retrieval. For cases with an average rain rate at the high end of the useful dynamic range, the scattering reduces the simulated rain rate as expected. This is because the FOV is partly covered by rainfall that is out of the useful dynamic range if the average rain rate is at the high end of the useful dynamic range. For cases with a very small average rain rate, scattering increases the simulated rain rate, even makes the simulated rain rate larger than the true rain rate. This is an artifact because the scattering effect is very small for light rain. In fact, the square

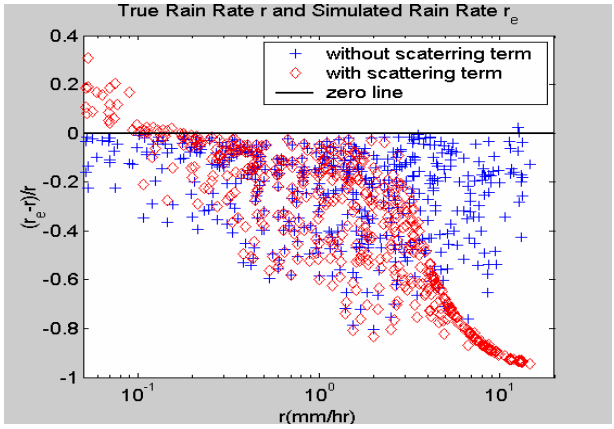

Fig. 24 Impact of scattering on beamfilling error for the TMI 37 GHz channel

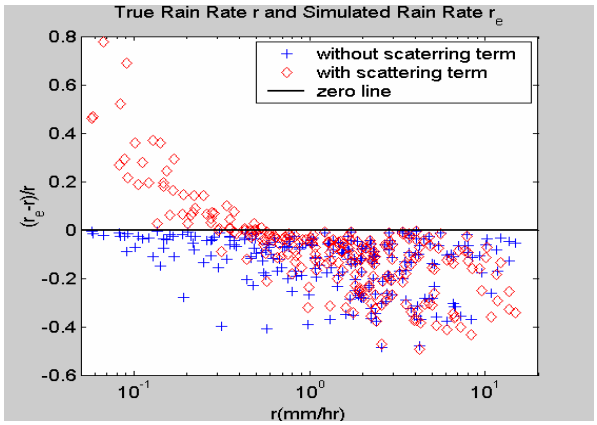

Fig. 25 Same as Fig. 24 except for the TMI 19 GHz channel

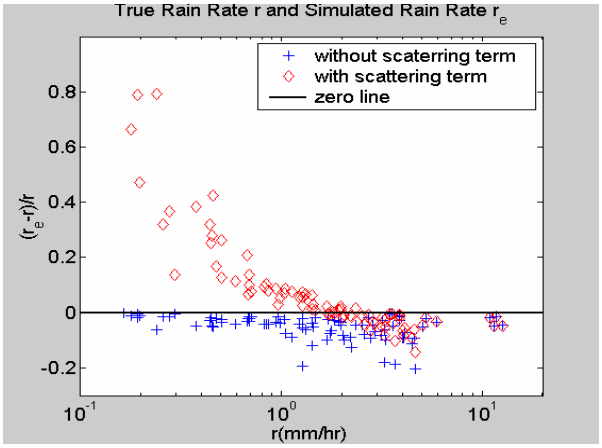

Fig. 26 Same as Fig. 24 except for the TMI 10 GHz channel

root term, $a\sqrt{R}$, can not represent the scattering accurately for light rain. The square root term changes the non-linearity of the R-T relation significantly in the small rain rate region. This is inappropriate. However, for 10 GHz and 19 GHz, this problem occurs at a rain rate where a higher frequency would be used, and for 37 GHz, it is only significant for rain rate of a few tenths of a mm/h or less.

5.2 Some Refinements to BCF Calculation

The characteristics of the previous algorithm for the BCF calculation are as follows:

1) Use A/C radar data to simulate the satellite observation. The simulation is based on the R– T relationship without the scattering term.
2) Do regression between the input rain rate and retrieved rain rate to find the BCF. The regression is based on all simulation results, the useful dynamic range is not considered.

According to the analysis in §5.1, the following refinements could make the BCF estimation closer to reality:

1) Scattering should be included in the simulation of satellite observations.
2) The BCF calculation should only include the cases that have average rain rates within the useful dynamic range of a channel.

KWAJEX ARMAR data are used to simulate TMI observations and estimate the BCF through the original algorithm and through the improved algorithm. Because the square root term, $a\sqrt{R}$, can not represent scattering accurately for very low rain rates, the cases with very low average rain rates are excluded for BCF estimation through the improved algorithm. Fig. 27 – Fig. 29 show the comparisons between the results of the

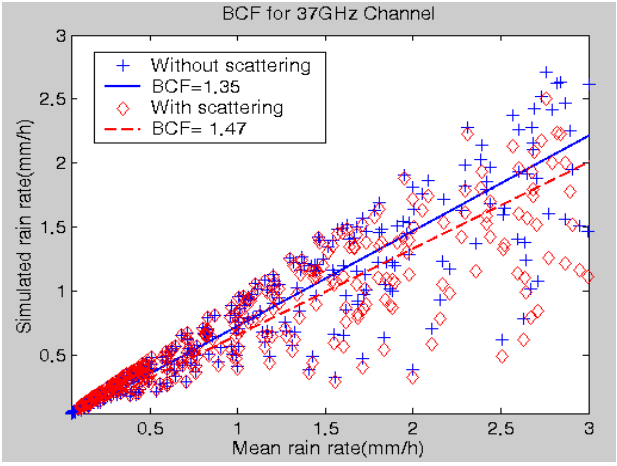

Fig. 27 Impact of scattering on BCF for 37 GHz

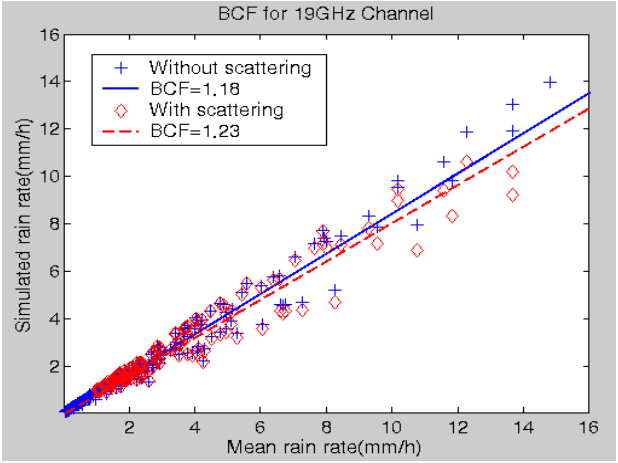

Fig. 28 Same as Fig. 27 except for 19 GHz

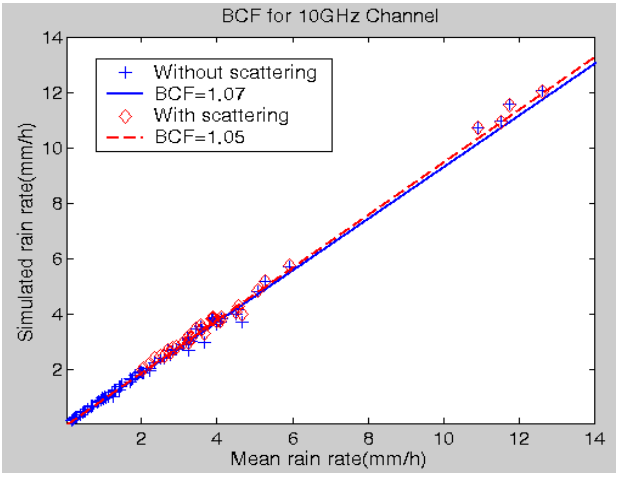

Fig. 29 Same as Fig. 27 except for 10 GHz

two algorithms. Compared to the original algorithm, the improved algorithm increases the BCF by 0.05 for the 19 GHz channel and by 0.12 for the 37 GHz channel, while there is no significant difference for the 10 GHz channel. This is consistent with the analysis in 5.1.

5.3 BCF as a Function of FOV Size

The BCF has a direct relation with rain rate variance over the FOV and the rain rate variance can be statistically expressed as a function of FOV size and average rain rate. Therefore, the BCF may be expressed as a function of FOV size, characteristic rain rate, and average rain rate. The combination of equation 2.4 and equation 3.5 yields:

$$BCF = 1 + 0.3136 \frac{\log_{10}^{2}(fov) R^{1.26}}{2 R_c R_e} C \qquad 5.1$$

where fov is the FOV size in the longer dimension. R is the average rain rate over the FOV. R_c is the characteristic rain rate . R_e is the estimated rain rate, which is almost proportional to R. C is a variable less than 1. Although there is no clear expression for C, from Fig. 4, C decreases as rain rate variance increases. Hence the effect of C and R_e may counteract the dependence of BCF on R. The real data simulation results, which are shown in Fig. 27, Fig. 28 and Fig. 29, also show that the BCF does not have much dependence on the average rain rate. In Fig. 27, there is some small dependence of the BCF on the average rain rate. This dependence is caused by scattering, which is not considered by equation 5.1. Scattering can increase the beamfilling error significantly for the 37 GHz channel and this becomes more obvious as the average rain rate over the FOV increases.

Equation 5.1 can not be directly applied to BCF estimation because it does not consider scattering and there is no clear expression for C. But from equation 5.1, the BCF depends significantly on the FOV size and the characteristic rain rate. The FOV size here means the FOV size in the longer dimension. The BCF has been estimated for various FOV sizes and characteristic rain rates. The results are shown in Fig. 30. The regression expresses BCF as a function of FOV size and characteristic rain rate:

$$BCF = 1 + 0.31\frac{\log_{10}^{2}(fov)}{R_c} \qquad 5.2$$

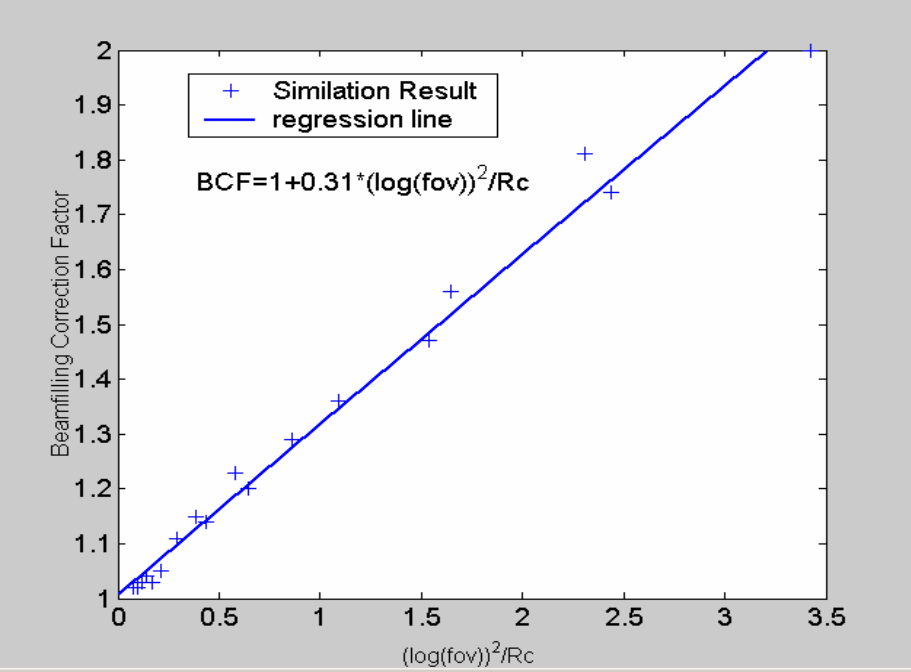

Fig. 30 Regression of BCF calculation result

CHAPTER VI

UNCERTAITY OF BCF

The available A/C radar data are limited compared to satellite spatial coverage and time coverage. Previously, only one specific data set has been used to correct satellite radiometer observations. Simulation results provide a BCF for global use. Even assuming the BCF is accurate in an average sense, it is inaccurate for individual FOVs. To understand the rainfall retrieval accuracy, the BCF error for each FOV in the data set should be estimated. This is called the local BCF uncertainty problem. Another problem is whether the BCF derived from a specific set of data can be used globally. In principle, the BCF we get is only reasonable for the time and location of the data used, even then only in a statistical sense. Usually the data set for BCF estimation contains a wide variety of rain types, but this wide variety of rain types are only in the location and duration of one field experiment. Rain characteristics change for different times and locations. The impact of these changes on the BCF should be estimated. This is called the global BCF uncertainty problem. The aim of this chapter is to estimate the uncertainty of the BCF both locally and globally.

6.1 Local BCF Uncertainty

Quantitative understanding of the BCF uncertainty must be based on real data. ARMAR data collected during KWAJEX and ARMAR data collected during TOGA/COARE are used to calculate BCF. Fig. 31- Fig. 36 show the BCF calculation results for KWAJEX ARMAR data and TOGA/COARE ARMAR data. The local BCF

uncertainty is shown in Table 6 for KWAJEX ARMAR data, and is shown in Table 7 for TOGA/COARE ARMAR data.

Table 6 Local BCF uncertainty derived from KWAJEX ARMAR data for TMI

Channel Frequency	FOV Size	BCF	STD of BCF error	Remarks
37 GHz	16 km	1.47	0.66	85%cases have BCF error within 0.47
19 GHz	30 km	1.23	0.20	86% cases have BCF error within 0.23
10 GHz	63 km	1.05	0.03	100% cases have BCF error within 0.05

Table 7 Same as Table 6 except from TOGA/COARE ARMAR data

Channel Frequency	FOV Size	BCF	STD of BCF error	Remarks
37 GHz	16 km	1.36	0.54	80%cases have BCF error within 0.36
19 GHz	30 km	1.20	0.20	89% cases have BCF error within 0.20
10 GHz	63 km	1.09	0.14	98% cases have BCF error within 0.1

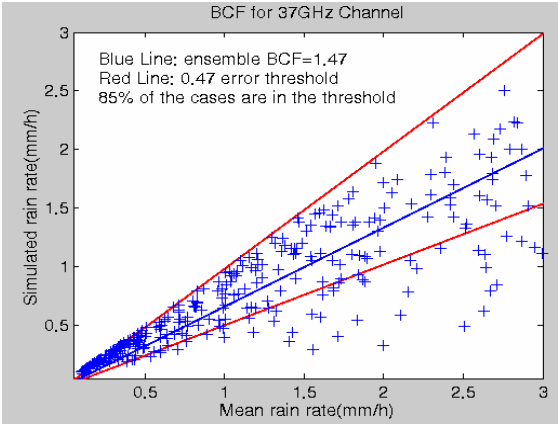

Fig. 31 Regression between true rain rate and simulated rain rate using KWAJEX ARMAR data for 37 GHz

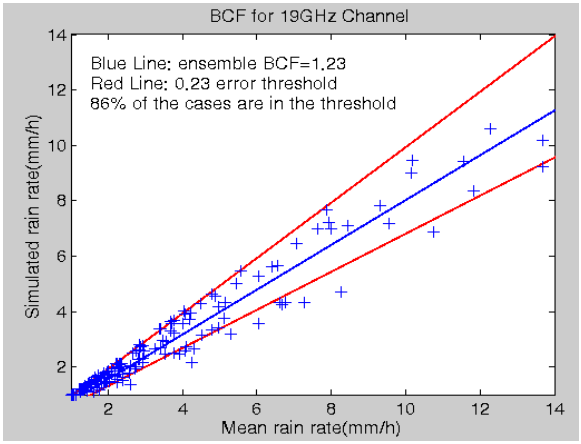

Fig. 32 Same as Fig. 31 except for 19 GHz

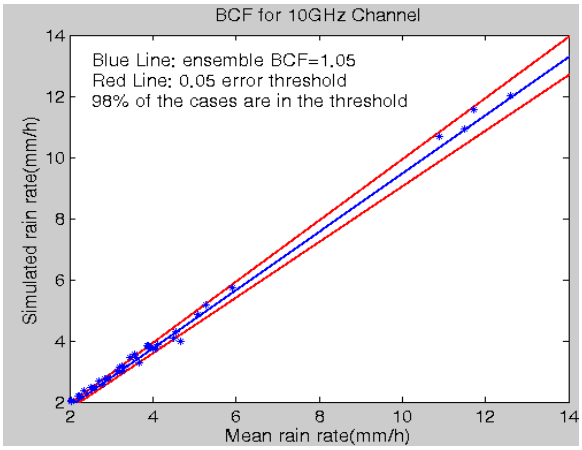

Fig. 33 Same as Fig. 31 except for 10 GHz

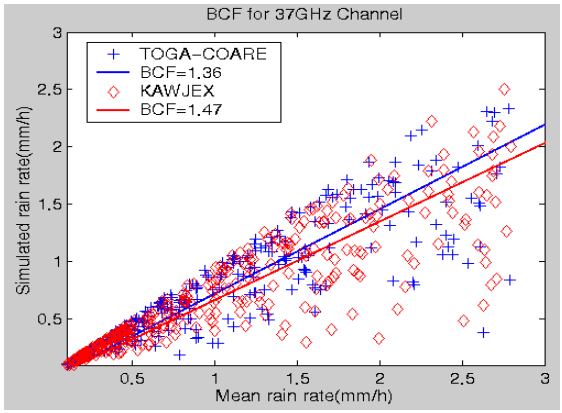

Fig. 34 Comparison of BCF calculation between TOGA/COARE ARMAR data and KWAJEX ARMAR data for 37 GHz

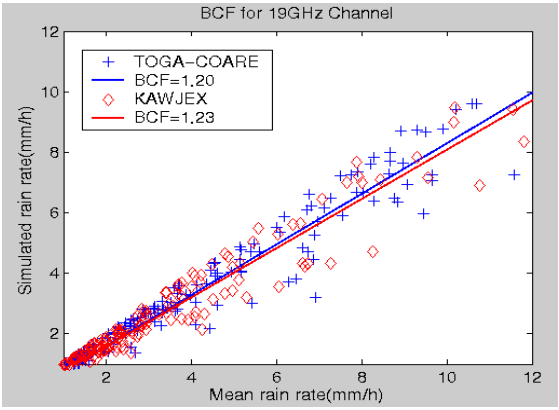

Fig. 35 Same as Fig. 34 except for 19 GHz

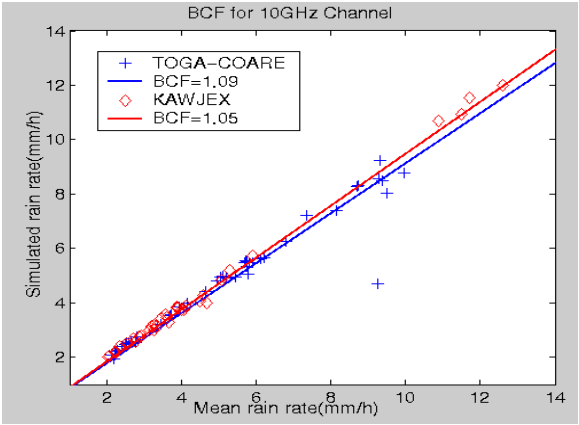

Fig. 36 Same as Fig. 35 except for 10 GHz

6.2 Global BCF Uncertainty

The TOGA/COARE and KWAJEX experiments were during different seasons and in different locations. The ARMAR collected a wide variety of rain types in both experiments. In chapter IV, the statistical characteristics of rainfall were found to be similar between the two experiments. This may mean that the statistical characteristics of rainfall over large spatial coverage and long time coverage does not change much for different locations and times, suggesting the same for the ensemble BCF. Fig. 34 – Fig. 36 show the comparison of BCF between TOGA/COARE and KWAJEX. From table 6 and table 7, compared with the BCF for KWAJEX, the BCF for TOGA/COARE is larger by 0.04 for the 10 GHz channel, is smaller by 0.03 for the 19 GHz channel and is smaller by 0.11 for the 37 GHz channel.

Ha and North (1995) studied the beamfilling error model and showed that beamfilling error uncertainty decreases as the FOV size and characteristic rain rate increase. According to their conclusion, generally speaking, compared with the higher frequency channels, the TMI 10 GHz channel should have smaller variability. In Fig. 36, there is an extreme case for TOGA/COARE ARMAR data. It contributes dominantly to the large BCF of TOGA/COARE for 10 GHz and makes the BCF difference between the two experiments larger than expected for the 10 GHz channel. But for the 19GHz channel and the 37 GHz channel, this extreme case is excluded because it is out of the useful dynamic range.

Based on the BCF comparison between KWAJEX and TOGA/COARE, the ensemble BCF does not change much for different locations and times. Hence the BCF derived from one specific set of data can be used globally. For example, if BCF for

KWAJEX is applied to TOGA/COARE data, the sum rain rate is overestimated by only 4 percent for the 10Ghz channel, is underestimated by only 3 percent for the 19 GHz channel and is underestimated by only 10 percent for the 37 GHz channel.

CHAPTER VII

SUMMARY AND CONCLUSION

Beamfilling error is one of the main error sources for microwave oceanic rainfall retrieval. An accurate beamfilling correction can improve the rainfall retrieval accuracy significantly. Quantitative understanding the uncertainty of the BCF is very important for the understanding of the accuracy of microwave passive rainfall retrieval.

BCF is determined by the rain rate distribution over the satellite FOV, channel frequency, freezing level and view angle. The rain rate distribution dominates the uncertainty of the BCF. Quantitative understanding the statistical characteristics of the rainfall distribution provides an indication of the beamfilling error and the uncertainty of the BCF in many ways. In this paper, the characteristics of rainfall distribution have been investigated using three-dimensional A/C radar data. Real data calculation shows that path averaging can reduce the variance of rain rate over the FOV significantly. The variance of rain rate over the FOV is summarized as a function of FOV size and average rain rate. The statistical characteristics of rain rate distribution have been found to be quite similar for rainfall during two different times and in two different locations. This suggests that the ensemble BCF is very stable.

All previous investigators dropped the scattering effect of rainfall for beamfilling error estimation because of its small contribution to the non-linearity of the R - T relationship. The scattering effect, however, acts as a dominant factor for heavy rain rates that are out of the useful dynamic range. It is possible that some part of a FOV may be covered by the rainfall that is out of the useful dynamic range while the average rain rate

over the FOV is within the useful dynamic range. If only the cases within the useful dynamical range are considered, scattering can increase the BCF by 0.12 for the 37 GHz, increase the BCF by 0.05 for the 19 GHz and has no obvious impact for the 10 GHz channel.

The available A/C radar data are limited compared to satellite spatial coverage and time coverage. Previously only one specific data set has been used to correct satellite radiometer observations. Simulation results provide a BCF for global use. Even assuming the BCF is accurate in an average sense, it is inaccurate for individual FOVs. In this paper, A/C radar data from the KWAJEX field experiment are used to investigate the uncertainty of the BCF for individual FOVs. It was found that 85% of the cases had BCF errors within 0.47 for the 37 GHz channel, 86% of the cases had BCF errors within 0.23 for the 19GHz channel, and 100% of the cases had BCF errors within 0.05 for the 10GHz channel.

Another problem is whether the BCF derived from a specific set of data can be used globally. In principle, the BCF we get is only reasonable for the time and location of the data used, even then only in a statistical sense. The TOGA/COARE and KWAJEX field experiments were during different seasons and in different locations. The comparison of the BCF between these two experiments can indicate the uncertainty of an ensemble BCF. Compared with the BCF for KWAJEX, the BCF for TOGA/COARE is larger by 0.04 for the 10 GHz channel, is smaller by 0.03 for the 19 GHz channel and is smaller by 0.11 for the 37 GHz channel. The values are much smaller than expected, showing that the BCF derived from a specific set of data can be used globally.

REFERENCES

Chiu, L. S., G. R. North, D. A. Short, and A. McConnel, 1990: Rain estimation from satellite: Effects of finite field of view. J. Geophy. Res., **95**, 2177-2185.

Durden, S. L., E. Im, F. K. Li, W. Ricketts, A. Tanner and W. Wilson, 1994: Armar: An airborne rain mapping radar, J. Atmos. Oceanic Tech., **11**, 727-737.

Ha, E., and G. R. North, 1995: Model study of the beam-filling error for rain-rate retrieval with microwave radiometers. J. Atmos. Oceanic. Technol., **12**, 268-281.

Hitschfeld, W., and J. Bordan, 1953: Errors inherent in the radar measurement of rainfall at attenuating wavelength. J. of Meteorology, **11**, 58-67.

Huang, J., 2001: An algorithm for retrieval of monthly rainfall over the oceans from the TRMM Microwave Imager(TMI), Ph.D Dissertation, Department of Atmospheric Sciences, Texas A&M University, College Station, TX, 100pp.

Iguchi, T. , and R. Meneghini, 1994: Intercomparison of single-frequency methods for retrieving a vertical rain profile from airborne or spaceborne radar data. J. Atmos. Oceanic Technol., **11**, 1507-1515.

Marecal, V., T. Tani, P. Amayenc, C. Klapisz, E. Obligis, and N. Viltard, 1997: Rain relations inferred from microphysical data in TOGA COARE and their use to test a rain-profiling method from radar measurements at Ku- Band. J. Appl. Meteor., **36**, 1629-1645.

Marshall, T. S., and W. Mck. Palmer, 1948: The distribution of raindrops with size. J. Meteor., **5**., 165-166.

Tanner, A., S. L. Durden, R. Denning, E. Im, F. K. Li, W. Ricketts and W. Wilson, 1994: Pulse compression with very Low sidelobes in an airborne rain mapping radar, IEEE Transaction on Geoscience And Remote Sensing, **32**, 211-213.

Wang, A., 1996: Modeling the beamfilling correction for microwave retrieval of oceanic rainfall, Ph.D Dissertation, Department of Atmospheric Sciences, Texas A&M University, College Station, TX, pp100.

Wilheit, T. T., A. T. C. Chang, M. S. V. Rao, E. B. Rodger and J. S. Theon, 1977: A satellite technique for quantitatively mapping rainfall rate over the oceans. J. Appl. Meteor., **16**, 551-560.

Wilheit, T. T., A. T. C. Chang and L. S. Chiu, 1991: Retrieval of monthly rainfall indices from microwave radiometric measurements using probability distribution functions. J. Atmos. Oceanic Technol., **8**, 118-136.

VITA

Ruiyue Chen was born in Chaohu, Anhui Province, People's Republic of China. He obtained his Bachelor of Science in electrical engineering in July, 1997 from Nanjing University of Aeronautics and Astronautics. He received his Master of Science in electrical engineering in March, 2000 from Nanjing University of Aeronautics and Astronautics. He was admitted to the Department of Atmospheric Sciences and joined the Microwave Remote Sensing Group in the fall of 2000 at Texas A&M University.

Correspondence may be addressed to:

Ruiyue Chen

200 Calvin Moore, #6F

College Station

TX, 77840